A Appendix

In the appendix, we provide the following materials:

- Training algorithm of DLoRAL (referring to Section 3.2 in the main paper);
- More ablation studies on training strategies and key components of DLoRAL (referring to Section 3.2 and Section 4.2 in the main paper);
- More real-world visual comparisons under scaling factor $4\times$ (referring to Section 4.2 in the main paper);
- Video demonstration;
- Broader impacts.

A.1 Training algorithm of DLoRAL

Algorithm 1 Training Algorithm of DLoRAL

Input: Training datasets $\mathcal{S}_{cons}$ and $\mathcal{S}_{enh}$, pretrained SD with VAE encoder E_ϕ, diffusion UNet ϵ_ϕ, and VAE decoder D_ϕ, cross-frame retrieval R, prompt extractor Y, training iteration N, consistency step N_{cons}, enhancement step N_{enh}.

Initialize two LoRA modules parameterized by θ_1 and θ_2 within diffusion UNet ϵ_ϕ, denoted as $\epsilon_{\{\phi,\theta_1,\theta_2\}}$
Initialize cross-frame retrieval module R parameterized by μ, denoted as R_μ
Initialize $N_{cycle} \leftarrow N_{cons} + N_{enh}$
for $i \leftarrow 1$ **to** N **do**
  if $(i-1) \bmod N_{cycle} < N_{cons}$ **then**
    /* Consistency Stage */
    Sample $\boldsymbol{x}_L, \boldsymbol{x}_H$ from $\mathcal{S}_{cons}$
    /* Network forward */
    $c_y \leftarrow Y(\boldsymbol{x}_L)$
    $\boldsymbol{z}_L \leftarrow E_\phi(\boldsymbol{x}_L)$
    $\hat{\boldsymbol{z}}_H \leftarrow \boldsymbol{\epsilon}_{\{\phi,\theta_1,\theta_2\}}(R_\mu(\boldsymbol{z}_L); c_y)$
    $\hat{\boldsymbol{x}}_H \leftarrow D_\phi(\hat{\boldsymbol{z}}_H)$
    /* Compute consistency loss group */
    $\nabla_{\theta_1}\mathcal{L}_{\text{data}} \leftarrow [\mathcal{L}_{\text{cons}}(\hat{\boldsymbol{x}}_H, \boldsymbol{x}_H)] \frac{\partial \hat{\boldsymbol{x}}_H}{\partial \theta_1}$
    $\nabla_{\mu}\mathcal{L}_{\text{data}} \leftarrow [\mathcal{L}_{\text{cons}}(\hat{\boldsymbol{x}}_H, \boldsymbol{x}_H)] \frac{\partial \hat{\boldsymbol{x}}_H}{\partial \mu}$
    /* Update parameters */
    Update θ_1 and μ with $\mathcal{L}_{\text{data}}$
  end
  else
    /* Enhancement Stage */
    Sample $\boldsymbol{x}_L, \boldsymbol{x}_H$ from $\mathcal{S}_{enh}$;
    /* Network forward */
    $c_y \leftarrow Y(\boldsymbol{x}_L)$
    $\boldsymbol{z}_L \leftarrow E_\phi(\boldsymbol{x}_L)$
    $\hat{\boldsymbol{z}}_H \leftarrow \boldsymbol{\epsilon}_{\{\phi,\theta_1,\theta_2\}}(R_\mu(\boldsymbol{z}_L); c_y)$
    $\hat{\boldsymbol{x}}_H \leftarrow D_\phi(\hat{\boldsymbol{z}}_H)$
    /* Compute enhancement loss group */
    $\nabla_{\theta_2}\mathcal{L}_{\text{data}} \leftarrow [\mathcal{L}_{\text{enh}}(\hat{\boldsymbol{x}}_H, \boldsymbol{x}_H)] \frac{\partial \hat{\boldsymbol{x}}_H}{\partial \theta_2}$
    /* Update parameters */
    Update θ_2 with $\mathcal{L}_{\text{data}}$
  end
end

Output: Generator G_θ including VAE encoder E_ϕ, cross-frame retrieval R_μ, latent diffusion UNet $\boldsymbol{\epsilon}_{\{\phi,\theta_1,\theta_2\}}$ and VAE decoder D_ϕ

[†]This work is supported by the PolyU-OPPO Joint Innovative Research Center.

A.2 More ablation studies on training strategies and key components of DLoRAL

Effectiveness of DLoRAL strategy. To validate the effectiveness of our proposed DLoRAL strategy, we first conduct ablation studies by testing three configurations: (a) using a single parameter space, where optimization is guided by consistency losses and enhancement losses simultaneously; (b) using a single parameter space with iterative optimization guided by consistency losses and enhancement losses; and (c) using a dual parameter space (*i.e.,* two LoRA modules), where optimization is guided by consistency losses and enhancement losses iteratively (referring to the settings in Section 3.3 of the main paper). To evaluate the video quality (measured by MUSIQ [1]) and temporal consistency (measured by warping error [2]) of the models at different training iterations, we conduct experiments on the VideoLQ4 subset, as described in the main paper. This subset consists of four representative sequences (013, 015, 020, and 041 clips), each with 100 frames, selected from the VideoLQ dataset to cover diverse scenes and motions. The results are shown in Fig. A1.

For the single parameter space optimized jointly, as illustrated in Fig. A1(a), the final performance is characterized by a relatively low warping error but poor image quality. During training, the decline in warping error is consistently accompanied by a degradation in image quality. Eventually, both warping error and image quality reach a bottleneck, highlighting the inherent difficulty of optimizing both objectives simultaneously. In contrast, the dual-stage training strategy, as illustrated in Fig. A1(c), achieves significantly better image quality while maintaining a comparable level of warping error. Although some conflicts between consistency and image quality remain in each stage, these conflicts diminish with iterations, as evidenced by the reduced warping error fluctuation (from 0.0013 in the first stage to <0.0005 in the second) and smoother MUSIQ improvement (stabilizing around MUSIQ = 66). These results demonstrate that the dual-stage strategy effectively mitigates conflicts and achieves a better balance between the two objectives.

Joint optimization guided by enhancement and consistency losses struggles to optimize both metrics simultaneously. To ensure a fair comparison, we also use a single parameter space with iterative optimization guided by consistency and enhancement losses, as illustrated in Fig. A1(b). The improvement in image quality is obtained at a price of significant increase in warping error, and vice versa. In addition, the similar performance between the first (*i.e.*, 0$\sim$5000 iterations) and second consistency stages (*i.e.,* 10000$\sim$15000) implies that the model may not fully utilize the priors from the intervening enhancement stage to improve the subsequent consistency stage. In contrast, DLoRAL, as shown in Fig. A1(c), leverages the priors learned from the previous stage as anchors, enabling effective information transfer and gradually mitigating conflicts. This allows DLoRAL to achieve significantly higher image quality while maintaining comparable warping error.

Effectiveness of each LoRA branch. To further clarify the roles of the two LoRA branches within our dual-stage framework, we conduct ablation studies by training three variants from scratch: (i) C-LoRA only, (ii) D-LoRA only, and (iii) the combined C+D configuration. Shown in Tab. A1, the results confirm that C-LoRA primarily enhances temporal consistency, while D-LoRA recovers fine spatial details; combining both yields the best overall performance. These findings substantiate the complementary contributions of each LoRA and justify the proposed dual-stage design.

	MUSIQ ↑	CLIP-IQA ↑	MANIQA ↑	E^*_{warp} ↓
C-LoRA only	50.5394	0.3052	0.2147	$\mathbf{1.48\times10^{-3}}$
D-LoRA only	65.8557	0.5420	0.3412	1.62×10^{-3}
C+D LoRA (Ours)	**66.6174**	**0.5475**	**0.3791**	1.51×10^{-3}

Table A1: Ablation study on the roles of each LoRA branch on the VideoLQ dataset.

Enhancement-stage first vs. consistency-stage first. For dual-stage training, an intuitive question arises: Should the first stage focus on detail enhancement or temporal consistency? We conduct experiments to answer this question with two options: an enhancement-first alternating strategy and a consistency-first alternating strategy. The quantitative and qualitative results are presented in Fig. A2 and Tab. A2.

As shown in Tab.A2 and Fig.A2, the enhancement-first model achieves comparable continuity but exhibits less details. This suggests that, although both configurations adopt the dual-stage alternating training strategy, the choice of the first stage impacts the final results. When the enhancement stage is used as the first stage, the model focuses on generating high-resolution details before optimizing the inter-frame warping error. However, the priors learned during the enhancement stage, which focus on

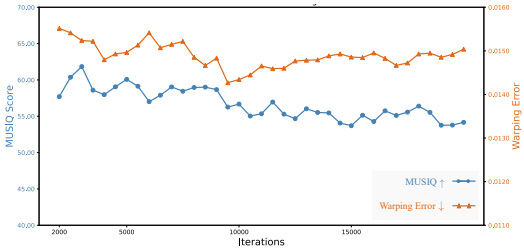

(a) Single parameter space and single stage

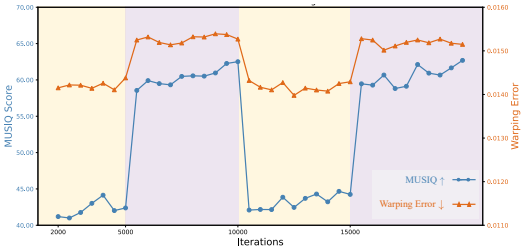

(b) Single parameter space and dual stages

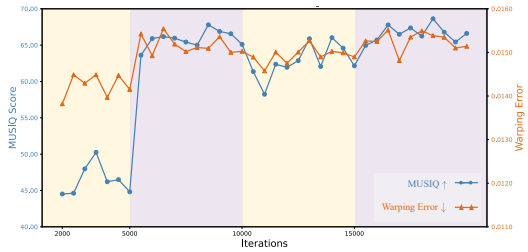

(c) Dual parameter spaces and dual stages

	MUSIQ ↑	Warping Error ↓
(a) Single parameter space and single stage	54.1642	1.5×10^{-3}
(b) Single parameter space and dual stages	62.6918	1.5×10^{-3}
(c) Dual parameter spaces and dual stages	66.6174	1.5×10^{-3}

(d) Final Result

Figure A1: Performance (MUSIQ [1] and Warping Error [2]) comparisons of different training strategies on the VideoLQ4 test dataset. (a) Joint optimization in a single parameter space struggles to balance image quality and temporal consistency, with both metrics reaching a bottleneck. (b) Iterative optimization fails to transfer priors effectively, leading to limited improvement. (c) In contrast, the dual-stage strategy mitigates conflicts and achieves superior image quality while maintaining comparable warping error. (d) Numeric results of the last iteration.

enhancing fine details, cannot be directly utilized as priors by the consistency stage, leading to certain degree of misalignment between the two stages. The misalignment consequently leads to poor image quality, as shown in Fig.A2. In contrast, when the consistency stage precedes the enhancement stage, it extracts temporal priors from degraded frames. The temporal priors serve as a foundation for the subsequent enhancement stage, leading to detail-rich and consistent outputs.

	MUSIQ↑	CLIPIQA↑	MANIQA↑	E^*_{warp}↓
Enhancement-first	49.484	0.299	0.258	7.040
Consistency-first	63.846	0.567	0.344	7.497

Table A2: Comparison of enhancement-first strategy and consistency-first strategy. The experiments are conducted on the VideoLQ dataset.

Temporal Window	**MUSIQ** ↑	CLIP-IQA ↑	MANIQA ↑	E^*_{warp} ↓
0 (w/o CFR)	64.5732	0.5148	0.3386	1.58×10^{-3}
1 (Ours)	**66.6174**	**0.5475**	**0.3791**	1.51×10^{-3}
3	65.4470	0.5452	0.3645	1.53×10^{-3}
5	62.1562	0.5019	0.3204	$\mathbf{1.50\times10^{-3}}$

Table A3: Ablation study on temporal window size in the CFR module. The experiments are conducted on the VideoLQ4 dataset

Analysis of CFR temporal design. We then analyze the impact of temporal window size in the Cross-Frame Retrieval (CFR) module. This experiment evaluates how different temporal receptive fields influence both visual quality and temporal coherence. Specifically, we vary the number of frames involved from 0 (*i.e.*, without CFR) to 5, with results shown in Tab. A3. We observe that a temporal window size of 1 achieves a good balance between temporal consistency and visual quality. When the temporal window is increased to 5, there is a slight drop in the warping error, indicating better temporal consistency. However, this comes at the cost of noticeably reduced visual quality, as reflected by the decrease in metrics such as MUSIQ and CLIP-IQA. On the other hand, when the temporal window is set to 0 (*i.e.*, without CFR), the warping error is significantly worse, highlighting

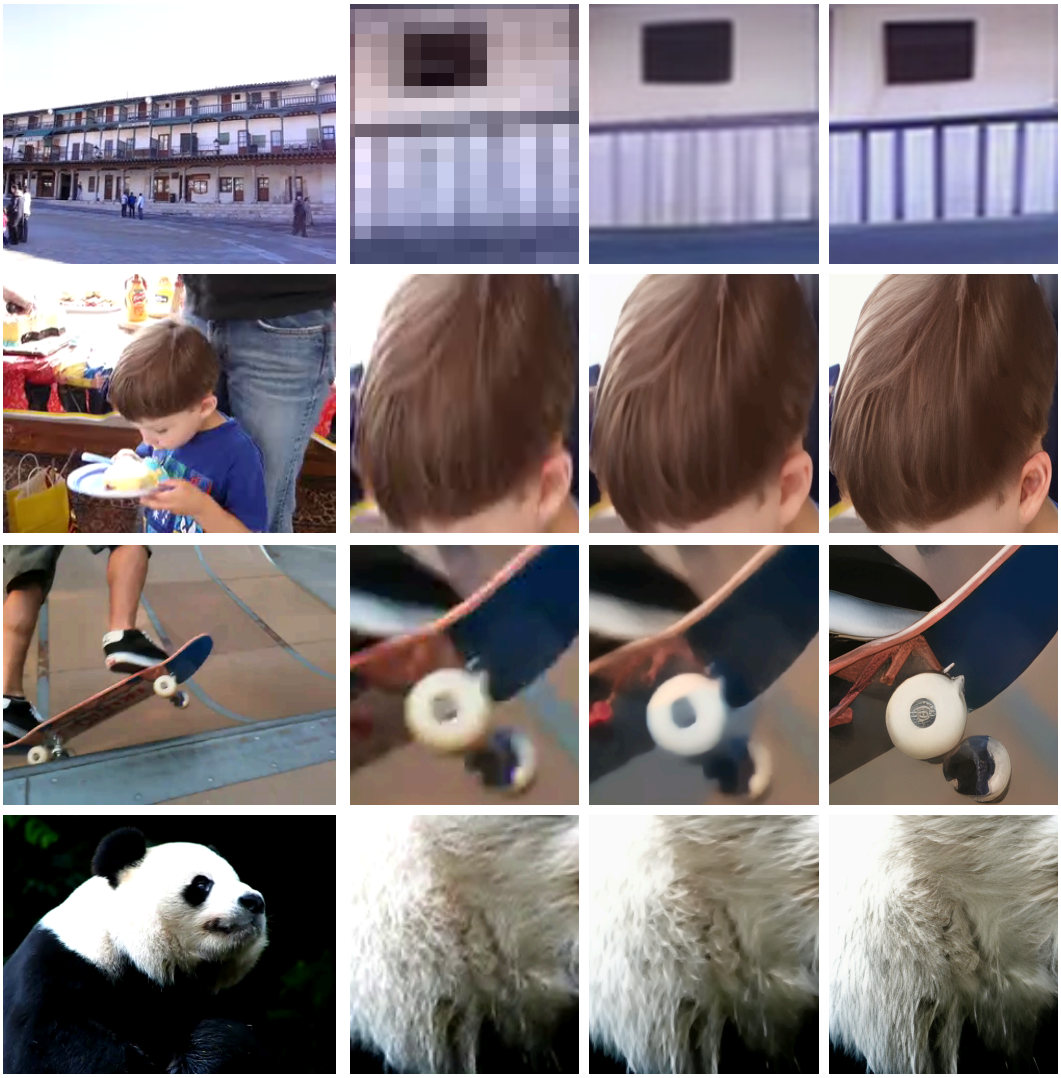

Figure A2: Visual comparisons of enhancement-first strategy and consistency-first strategy. The experiments are conducted on the VideoLQ dataset.

the importance of cross-frame interactions introduced by the CFR module. We adopt a temporal window of 1 in our final design for the trade-off in visual quality and computational efficiency.

A.3 More visual comparisons

Fig. A3 provides more visual comparisons between DLoRAL and other diffusion-based Real-VSR methods. DLoRAL achieves better results in preserving complex textures such as animal fur, plants, and buildings.

A.4 Video demonstration

We provide a demonstration video (**DLoRAL.mp4**) at `https://drive.google.com/file/d/1mwNRKo7SaJkezjptE4PctfKjx4VGNJNc/view?usp=sharing` to illustrate the effectiveness of our method on real-world video inputs, particularly highlighting its temporal coherence and high-fidelity detail preservation. Note that the videos are compressed and the original results exhibit higher visual quality. To ensure optimal visual perception and fair comparison of fine structures, please view the videos at 1080p resolution.

A.5 Broader impacts

This paper presents an exploratory study on real-world video super-resolution using one-step diffusion model. The main academic contribution is to advance video super-resolution research and inspire new methods in related fields. In terms of broader societal impact, the proposed method can significantly improve the quality of videos captured by cameras and mobile devices, with potential benefits for areas such as remote education and digital content creation. While higher-quality media may increase data storage demands, these challenges are manageable and outweighed by the advantages of enhanced video resolution.

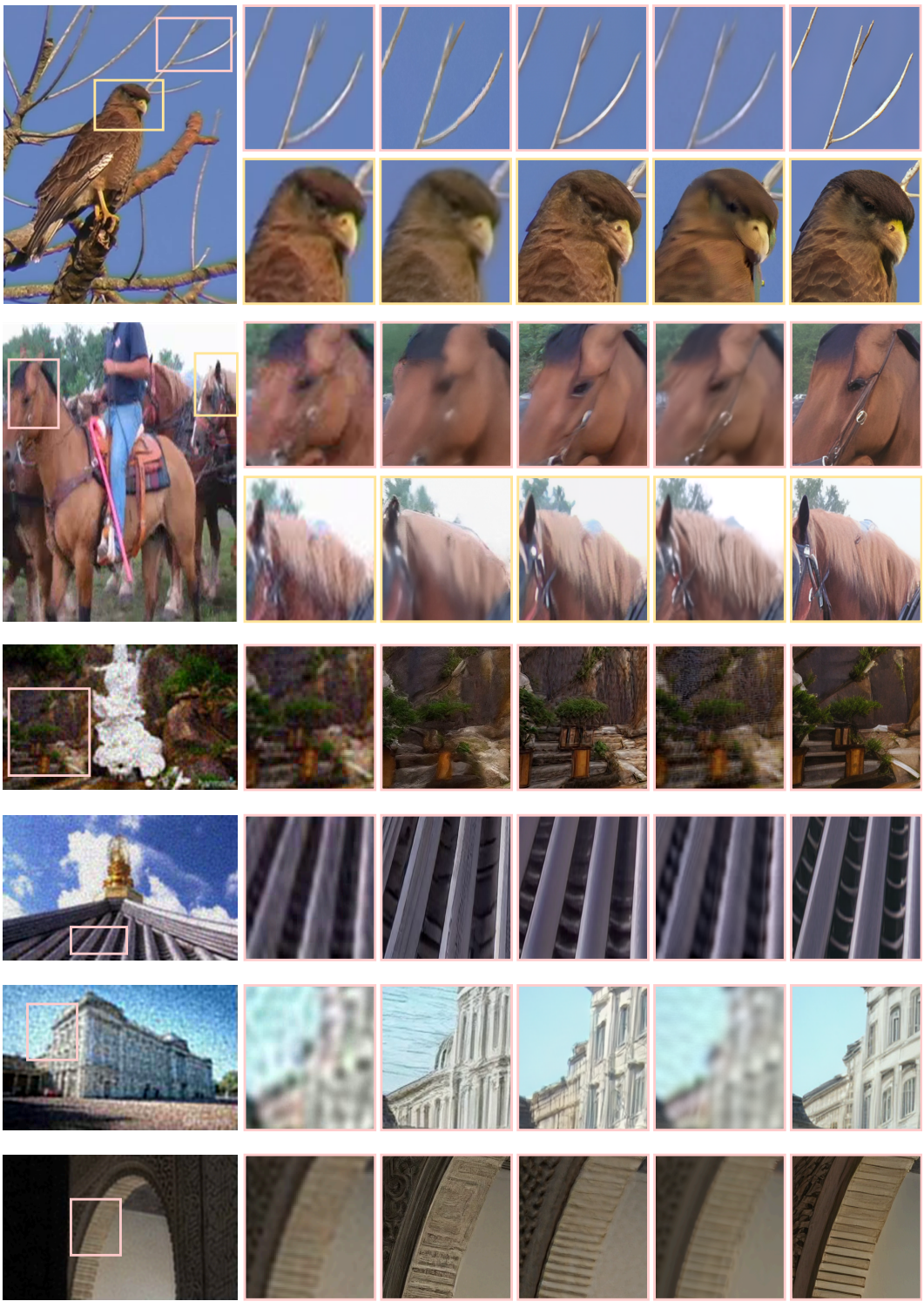

Figure A3: More Visual Comparisons of diffusion-based Real-VSR models on real-world and synthetic datasets. Please zoom in for a better view.

References

[1] Junjie Ke, Qifei Wang, Yilin Wang, Peyman Milanfar, and Feng Yang. Musiq: Multi-scale image quality transformer. In *Proceedings of the IEEE/CVF international conference on computer vision*, pages 5148–5157, 2021.

[2] Xi Yang, Chenhang He, Jianqi Ma, and Lei Zhang. Motion-guided latent diffusion for temporally consistent real-world video super-resolution. In *European Conference on Computer Vision*, pages 224–242. Springer, 2024.